Research Article GU J Sci 37(2): 677-686 (2024) DOI: 10.35378/gujs.1279556

Gazi University

Journal of Science

http://dergipark.gov.tr/gujs

A Low-Profile High Isolation Wideband Dual-Polarized Antenna for Sub-1 GHz Base Stations

Emre A. MIRAN[1*], Mehmet CIYDEM[2]

[1]*ESEN System Integration, 06800, Ankara, Türkiye*
[2]*Department of Electrical and Electronics Engineering, Gazi University, 06560, Ankara, Türkiye*

Highlights

- This paper focuses on design of a dual-polarized antenna for sub-1 GHz base stations.
- Crossed-slots in elliptic form are used for the excitation of the suspended stacked patch antenna.
- A wideband antenna with low-profile and high isolation is achieved for the desired performance.

Article Info

Received: 08 Apr 2023
Accepted: 24 July 2023

Keywords

Dual-Polarization
High-Isolation
Wideband
Crossed-Slot Coupling
Base Station Antenna

Abstract

This study introduces a compact, wideband dual-polarized suspended patch antenna designed for LTE700/LTE850/CDMA850/GSM900 applications, with a focus on achieving high isolation. The antenna design has two suspended patches that are excited in orthogonal directions using a modified crossed-slot configuration. The modifications applied to the crossed-slot significantly enhance the −15 dB impedance bandwidth, resulting in improved port isolation between polarizations. Both theoretical analysis and experimental testing confirm these enhancements, revealing an impressive −15 dB impedance bandwidth of 37% (688-1000 MHz) and port isolation exceeding 35 dB in the operating band. The antenna exhibits symmetric and directional radiation patterns in principle planes, with half-power beamwidths ranging from 55.32º to 65.61º and 61.79º to 66.84º. Antenna gain show exhibits variation in the range of 7.3-8.4 dBi across the measured frequencies. The compact size of the antenna, measuring 380 × 380 × 43.6 mm³, makes it highly suitable for integration into commercially deployed base stations. Throughout the paper, we provide a detailed presentation of the antenna's geometry, feeding mechanism, parametric studies, and experimental results. The combined theoretical analysis and practical experimentation validate the success of the proposed antenna design, highlighting its potential for robust performance in a wide range of communication applications.

1. INTRODUCTION

The continuous growth of mobile telecommunication technologies has made it inevitable that the communication networks operating in different bands must be used simultaneously. Consequently, there is a high demand for wideband antennas that can cover these diverse bands effectively at base stations. In particular, the low frequency range of 698-960 MHz is of significant importance as it includes several commercial sub-bands like LTE700 (698-746 MHz), LTE850 (814-894 MHz), CDMA850 (825-880 MHz), GSM900 (889-960 MHz), and others. Within this frequency range, the challenges lie not only in achieving wide operational bandwidth but also in designing base station antennas that are physically compact and space-efficient. Researchers have been working on solutions for developing wideband antennas that do not rely on complex feeding configurations or bulky structures. The aim is to simplify the manufacturing process and enhance system integration. By addressing these challenges, the industry can more effectively meet the requirements of modern communication systems that operate seamlessly across multiple frequency bands.

Recently, wideband antennas with dual polarization have gained popularity in commercial base stations due to their ability to offer polarization diversity and enhance channel capacity [1-3]. As a result of their

*Corresponding author, e-mail: alp.miran@esensi.com.tr

successful implementation in cellular communication systems, these antennas have seen broader adoption, now covering the entire sub-1 GHz band (698-960 MHz). Notably, these antennas are recognized for their multiband operation capabilities, all the while maintaining a high level of polarization isolation.

In the literature, the wideband dual-polarized type base station antennas, covering 698-960 MHz band, can mainly be investigated in two subcategories: crossed-dipole antennas [4-10] and planar patch antennas [11-21]. The design of the crossed-dipole antennas is mostly realized by a pair of two separate dipoles mounted in ±45º slanted placement. In [4-7], multiband crossed-dipole antennas operating in both 698-960 MHz and 1710-2690 MHz bands are proposed. In [4], the proposed antenna provides 18% VSWR > 1.5 in 800-960 MHz band with an average port isolation of 20 dB. [5] presents a dual polarized antenna of which vertical polarization (VP) operates in 806-960 MHz band with 17.4% −15 dB bandwidth whereas its horizontal polarization (HP) covers 1880-2700 MHz band. Similarly, in [6], VP of the proposed antenna exhibits −10 dB impedance bandwidth in 780 - 960 MHz. Since VP and HP of the antennas given in [5-6] operate in separate frequency bands, port isolation is not considered for these antennas. In [7], a printed dipole with dual polarization and operating in triple-band is proposed. The antenna spans 700-960 MHz band with 31.3% −10 dB impedance bandwidth and with more than 27 dB port isolation. Note that the multiband operation of these antennas relies on complicated feeding structures alongside inevitably high profiles. In [8-10], single band dual-polarized crossed-dipole antennas which operate along 698-960 MHz band are studied. [8] reports a compact crossed-dipole antenna with balun structure. The antenna exhibits VSWR < 1.5 and port isolation stronger than 26 dB. Although the size of the antenna is reduced by using bent dipoles, it still possesses high profile. In [9], a high isolation antenna containing a pair of printed planar dipoles is presented. The antenna is capable of providing 22.7% VSWR < 1.5 in 575-722 MHz band and port isolation more than 35 dB. He et al. presented a wideband crossed-dipole antenna in [10] which spans entire 698 - 960 MHz frequency band with the VSWR < 1.7. However, its port-to-port isolation is around 25 dB which is lower for common crossed-dipole antennas operating as base station antennas. Although the crossed-dipole configuration provides comparably good electrical performance in terms of wideband operation and port isolation, their profile height makes them unpractical for base station applications, especially in low frequencies.

The planar patch type antennas are practically adapted for base station applications because of their low profile, compactness and fabrication. The wideband operation of such antennas is realized mostly by either probe feeding or slot coupling techniques. In [11], a dual-polarized crossed-slot coupled suspended patch antenna, namely X-polar antenna, is demonstrated for 790-980 MHz operation. The proposed antenna yields −14 dB in-band impedance bandwidth and average 30 dB port isolation. In [12], the antenna structure given [11] is upgraded for dual band operation covering both 790-960 MHz and 1710-2180 MHz bands with no apparent performance improvement in the lower band. A tunable dual-polarized microstrip patch antenna with cavity-backing is demonstrated in [13]. The antenna has 0.9% and 1.8% −10 dB impedance bandwidths at 600 MHz and 1000 MHz, respectively. Despite its very low profile and compactness, the proposed antenna covers very narrow bandwidth (from 5.4 MHz to 18 MHz) at any tuned resonant frequency in its range. A wideband patch antenna fed by L-shaped probes is presented in [14]. It is designed for GSM900 and provides 18% −14 dB impedance bandwidth and 30 dB port isolation. Modified versions of [14] are presented by [15-18] at higher frequency bands. In [19], elliptic-shaped slot is introduced in order to create an ultra-wideband transition between microstrips in vertical direction. It is theoretically described and experimentally validated that axial ratio of the ellipse significantly increases amount of electromagnetic power that is transferred between the microstrips. In our study, this concept is further extended and considered for excitation mechanism of the patch antenna which usually suffers narrow impedance bandwidth. Employment of elliptic crossed-slot with patch antennas has also been studied for 5G applications in sub-6 GHz band [20, 21].

In this paper, a compact, low profile, slot-coupled dual-polarized wideband suspended patch antenna is proposed for base station applications in 698-960 MHz. The antenna radiates from two patches: Main patch and parasitic patch. The patches are excited through a modified crossed-slot which mainly grants the antenna's wide operational bandwidth, high isolation, and ±45º polarization diversity. The proposed antenna is able to maintain 37% −15 dB impedance bandwidth (688 - 1000 MHz) and more than 35 dB port isolation along the intended bandwidth. In addition, the antenna provides symmetric broadside radiation

patterns with 55.32º-65.61º and 61.79º-66.84º in principle planes. The antenna gain is 7.85 ± 0.55 dBi. The experimental results show that the proposed antenna meets the requirements of LTE700/LTE850/CDMA850/GSM900 band applications.

2. MATERIAL METHOD

2.1. Antenna Geometry

Figure 1 displays the geometry of the proposed antenna which composed of a feeding layer and two suspended square patches. The feeding layer is realized on FR4 (ε_r = 4.4, tanδ = 0.02) with 1.6 mm thickness. The bottom of the feeding layer contains the feeding network while its topside is kept as the common ground of size 380 × 380 mm^2 where the crossed-slot is etched. The main patch of length L_{mp} and the parasitic patch of length L_{pp} are appropriately mounted on the feeding layer by separators of specific heights of h_{mp} and h_{pp}, respectively. All physical parameters of the design are given in Table 1.

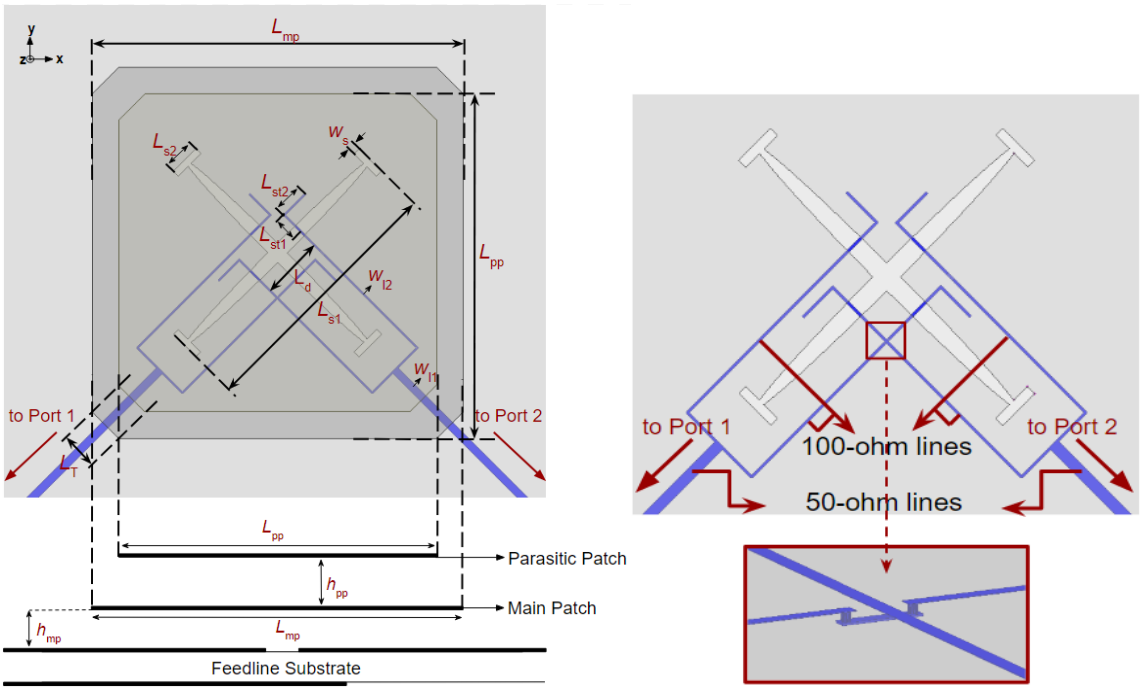

Figure 1. *Proposed antenna a) geometry, b) feeding configuration*

2.2. Working Principle

The fundamental principle of the proposed antenna relies on integrating a slot-coupled feeding mechanism into the suspended patch configuration. The slot features modified H-slots symmetrically positioned in a ±45º slanted configuration. Unlike typical rectangular-shaped H-slots, the middle part of the slot is elliptical in shape. This adjustment significantly enhances the antenna's impedance bandwidth and improves the isolation between the input ports. Axial ratio of elliptic curve, particularly the length of its axis, has a crucial role in determining the amount of electromagnetic power coupled to the patches.

Figure 1 illustrates the delivery of electromagnetic power from 50 Ω SMA ports to the slot through symmetric microstrip lines. Each slot is driven by two 100 Ω microstrip branches, separated by a distance of L_d, and loaded by L-shaped stubs to compensate the reactive part of the equivalent input impedance of the patches, $Z_{in,p}$. To ensure smooth line-crossing where the inner branches overlap, an air bridge is introduced. The branches are then combined and connected to the main 50 Ω feedline using a T-junction. Notably, the widths of the lines are calculated based on their impedances at the operating center frequency, f_c = 830 MHz (λ_c = 36.14 cm), and are listed in Table 1.

Table 1. *Antenna dimensions*

Description	Parameter	Dimension (mm)
Main patch (square) length, height	L_{mp}, h_{mp}	140, 18
Parasitic patch (square)	L_{pp}	120
Separation between patches	h_{pp}	22
Slot length	L_{s1}	99
Vertical slot length	L_{s2}	12
Stub width	w_s	2.6
Patch edge cut	L_T	14.14
Stub length #1, #2	L_{st1}, L_{st2}	8.55, 10.9
50 Ω / 100 Ω microstrip line width	w_{l1}, w_{l2}	2.96, 0.67
Branch Separation	L_d	12
Conductor thickness	t	0.035
FR4 height	h	1.6
Ground plane (square)	L_g	380

The patches utilized in this study are made of galvanized sheets with a thickness of 0.5 mm. It is preferred to avoid printing the patches on a dielectric layer to eliminate dielectric losses. Current distributions on the patches at 700 MHz and 900 MHz, while exciting the antenna from port 1 (+45º polarization), are depicted in Figure 2. At 700 MHz, the amplitude of the current distribution on the main patch starts to increases from the center towards the radiating edges in symmetry with the +45º plane, while the currents on the parasitic patch remain weak with a uniform distribution. As the frequency increases to 900 MHz, stronger coupling occurs between the two patches, resulting in an increase in the current amplitudes flowing on the parasitic patch. This phenomenon gives rise to resonant behavior around 900 MHz. Moreover, the symmetry observed along the +45º diagonal plane contributes to a low cross-polarization level in the far-field.

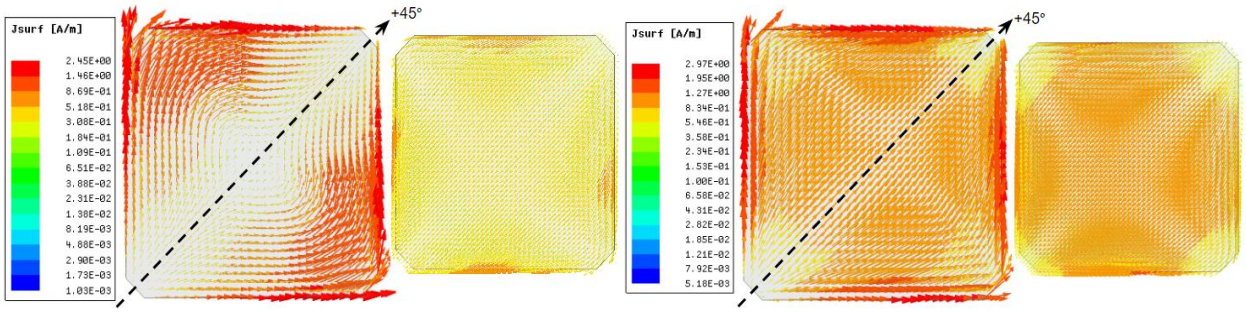

(a) *(b)*

Figure 2. *Current distribution on the main and parasitic patches at (a) 700 MHz and (b) 900 MHz*

2.3. Numerical Analysis

In favor of investigating the working principle and acquiring the optimal electrical performance, the proposed antenna is modeled and parametrically studied in finite element method based Ansoft HFSS. At each step of the parametric studies, effect of only one parameter is analyzed by sweeping within a specific range as the rest of the antenna is kept physically unchanged. The analysis results are provided by return loss ($|S_{11}|$) and isolation graphs ($|S_{21}| = |S_{12}|$) to illustrate the effect of the changes in parameters. Due to symmetry, results for 2nd port ($|S_{22}|$) are not given.

The height of the main patch, denoted as hmp, is a crucial factor influencing the performance of the proposed antenna. Figure 3 illustrates the |S11| and |S21| responses to variations in h_{mp}. As h_{mp} increases from 12 mm to 24 mm in 3 mm increments, there is a steady improvement in the −15 dB impedance bandwidth and port isolation until h_{mp} reaches 18 mm. At h_{mp} = 18 mm, the antenna gives an impressive

−15 dB impedance bandwidth of 39.92% and maintains a port isolation level exceeding 35 dB across the frequency band. However, for h_{mp} values greater than or equal to 21 mm, the −15 dB impedance bandwidth gradually narrows down, and the port isolation level diminishes. As h_{pp} (height of the parasitic patch) exhibits a similar impact as h_{mp}, its results are not included in this paper.

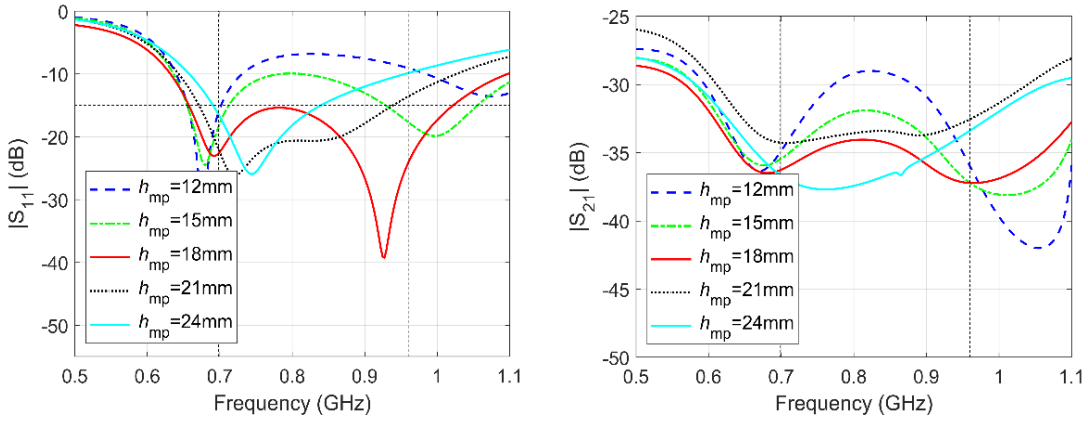

(a) *(b)*

Figure 3. *Effect of h_{mp} (a) reflection, $|S_{11}|$ and (b) isolation, $|S_{21}|$*

The precise positioning of the slot's excitation is critical for slot-coupled antennas because the impedance of the slot varies along its horizontal dimension concerning the current and voltage distributions on it. Therefore, the parameter L_d plays a significant role in determining the antenna's performance. Figure 4 illustrates the |S11| and |S21| responses as L_d varies. By sweeping L_d from 9 mm to 15 mm in 3 mm increments, the antenna achieves its widest −15 dB impedance bandwidth and highest matching level across the operating frequency band when L_d is set to 12 mm. At this value, port isolation is typically over 35 dB, showcasing the favorable performance of the antenna.

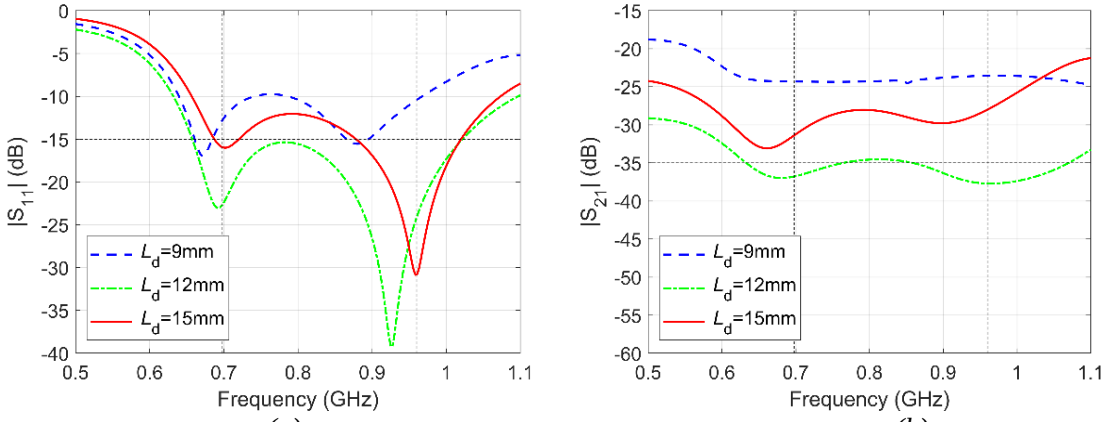

(a) *(b)*

Figure 4. *Effect of L_d (a) reflection, $|S_{11}|$ and (b) isolation, $|S_{21}|$*

Figure 5 depicts $|S_{11}|$ and $|S_{21}|$ characteristics of the proposed antenna regarding axial ratio of elliptic part of the slot, A_{xl}. It is swept within 34-42 by step of 4. When A_{xl} = 38, the antenna provides 40.07% −15 dB impedance bandwidth and the strongest port isolation over the intended frequency band.

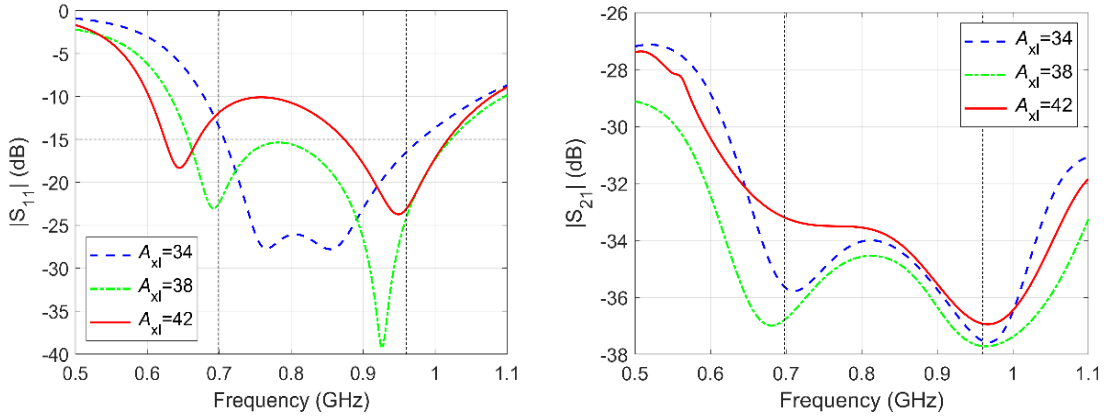

(a) *(b)*

Figure 5. *Effect of A_{xl} (a) reflection, $|S_{11}|$ and (b) isolation, $|S_{21}|$*

The advantage of the ellipse-shaped slot on the performance of the proposed antenna is investigated by comparing it with a rectangular-shaped H-slot of the same length (L_{s1} = 99 mm) and area size (A_s = ~404 mm^2). The results of this comparison are plotted in Figure 6. It can be observed that the elliptic-shaped H-slot improves matching level and exhibits wider −15 dB impedance bandwidth than rectangular-shaped H-slot. Investigation of the port isolation levels is also shown by the current distributions around slots. Amplitude of the currents is lower around the center in elliptic-shaped H-slot case which indicates lower coupling and stronger isolation between the polarizations.

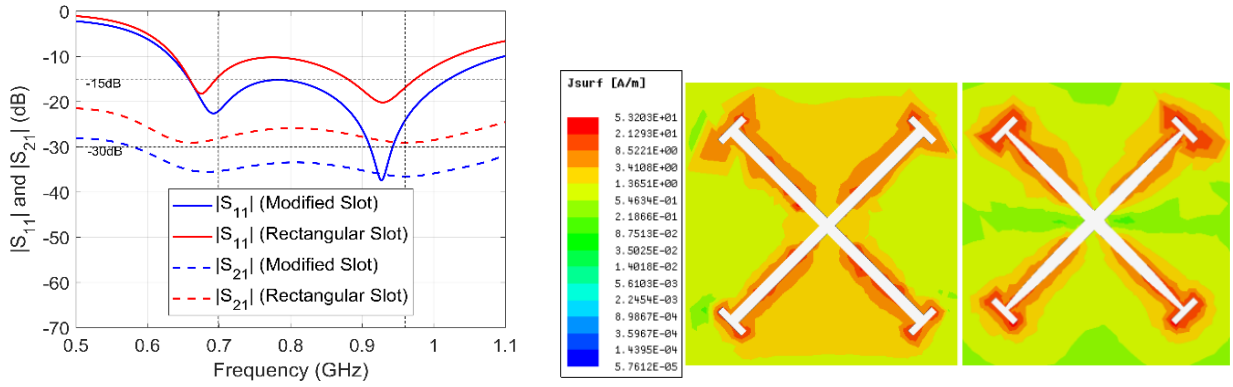

(a) *(b)*

Figure 6. *Comprison of the modified slot to the conventional rectangular-H slot in terms of a) s-parameters, b) current distribution on the ground*

Note that rest of the parameters is also numerically analyzed to examine their contribution to the antenna's performance. However, their results are not included in this paper because they do not create a significant enhancement on the electrical properties of the antenna. In the final design of the antenna, these parameters are optimized for the best performance.

3. THE RESEARCH FINDINGS

The proposed antenna is validated and tested by fabricating a prototype as described through section 2. The overall size of the prototype is 380 × 380 × 42.6 mm^3 and its photograph is given in Figure 7. The 2-port scattering parameter measurements ($|S_{11}|$, $|S_{21}| = |S_{12}|$, $|S_{22}|$) are carried out by a Hewlett-Packard 8720D vector network analyzer.

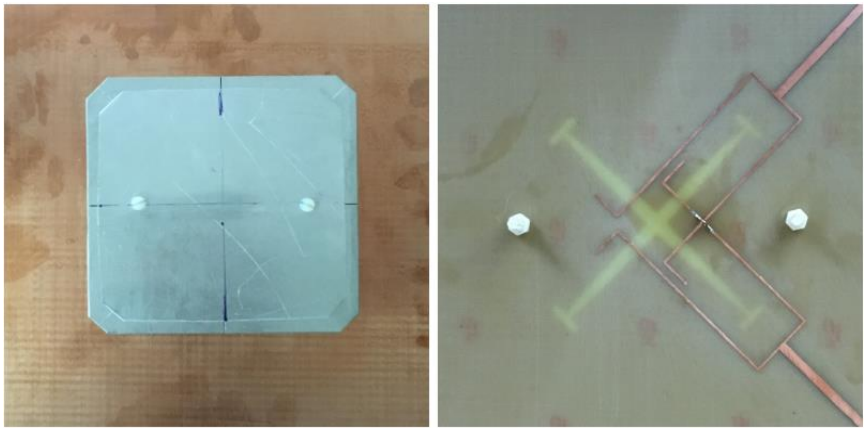

(a) *(b)*

Figure 7. *Antenna prototype (a) top view, (b) bottom view*

Figure 8 plots $|S_{11}|$ and $|S_{21}|$ graphs of the prototype. The graphs reveal that the antenna is capable of achieving about 37% (in 688-1000 MHz band) −15 dB impedance bandwidth (47.8% −10 dB impedance bandwidth). The discrepancies, which are quite small, between the simulated and the measured results comes from the fabrication tolerances, however the antenna still presents wideband operation as intended. The typical port isolation of the antenna is above 35 dB. The maximum isolation is recorded as around 70 dB.

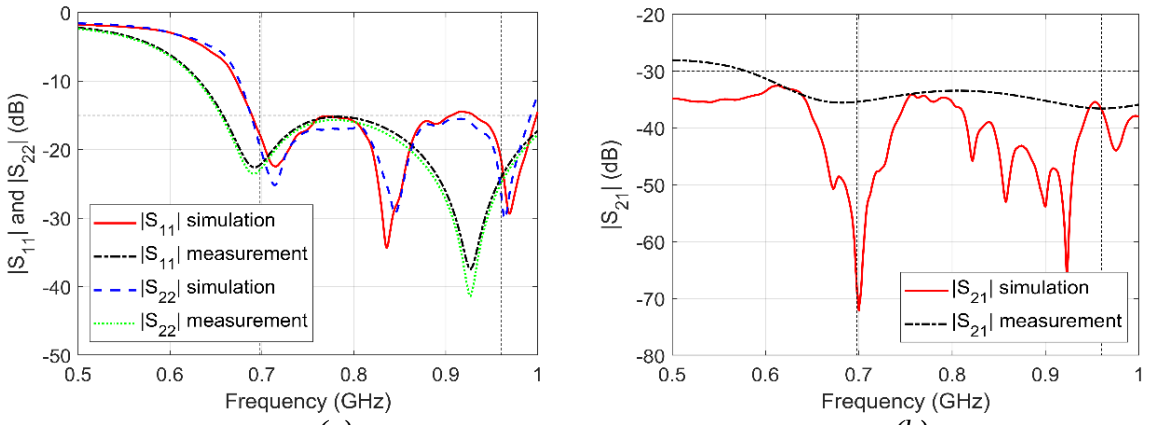

(a) *(b)*

Figure 8. *Comparison of the simulated and the measured s-parameters. a) $|S_{11}|$, $|S_{22}|$, and b) $|S_{21}| = |S_{12}|$*

Radiation pattern measurements for co/cross polarization components are conducted in an anechoic chamber using a computer-controlled graphical user interface. To prevent interference from unwanted scattered waves, the antenna is mounted on a foam block within the chamber. The measurements are obtained with the antenna excited from port 1 (+45º polarization) and with the other port terminated by a wideband 50 Ω load. Owing to its symmetric geometry, results obtained from exciting the antenna in the −45º configuration are not included in this paper. Figure 9 illustrates the stable and symmetric broadside radiation patterns of the antenna across the 698-960 MHz band. The measured co-polar half-power beamwidths (HPBWs) in the elevation plane are 65.61º, 60.94º, and 55.32º at 700 MHz, 825 MHz, and 950 MHz, respectively. In the azimuth plane, the measured co-polar HPBWs are 66.84º, 64.50º, and 61.79º. The front-to-back ratio (FBR) of the antenna consistently exceeds 27.97 dB on average. Moreover, the average cross-polarization discriminations (XPDs) are measured above 25 dB at boresight and below 29 dB at ±60º. Antenna measured gain changes from 7.3 dBi to 8.4 dBi over the corresponding frequency band.

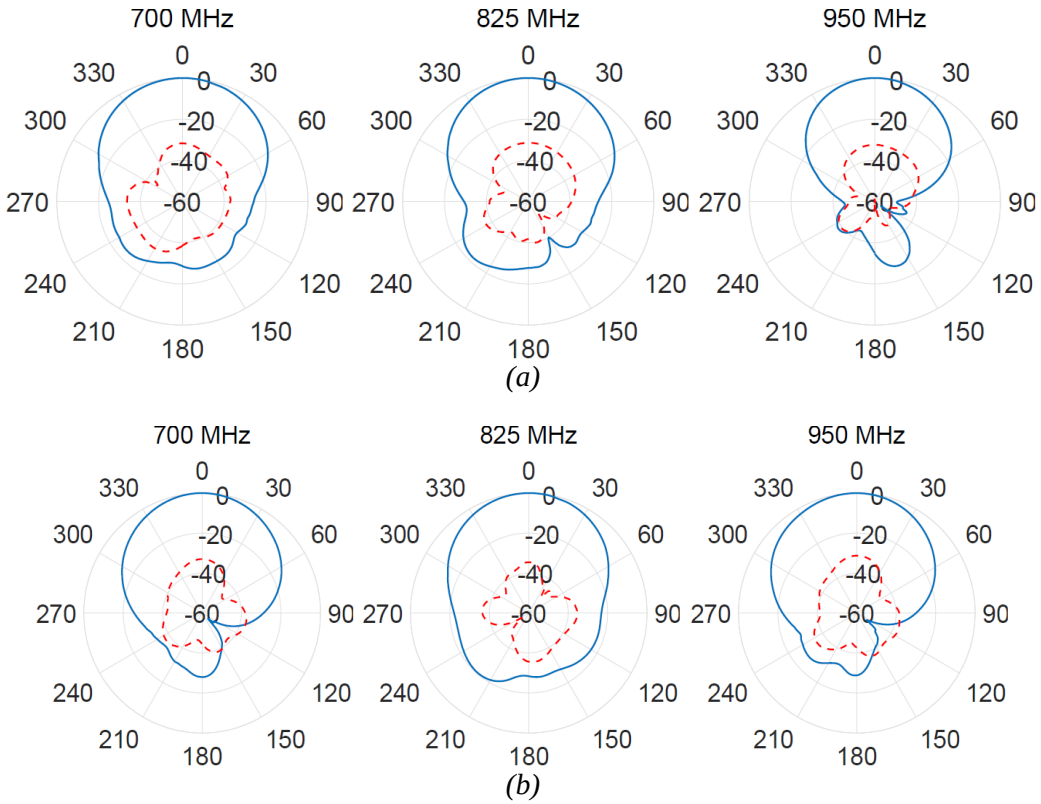

Figure 9. *Co-pol (solid blue line) and cross-pol (dashed red line) radiation patterns (a) in elevation and (b) in azimuth planes at corresponding frequencies*

4. RESULTS

In this paper, we have presented a low-profile, wideband suspended patch antenna with ±45º polarization diversity. The antenna's compact size, measuring 380 × 380 × 43.6 mm³, features a straightforward structure that facilitates easy fabrication. Excitation of the antenna utilizes a modified slot-coupling technique, which has been both numerically and experimentally validated to enhance the impedance bandwidth and improve port isolation. Specifically designed for base station applications, the antenna covers LTE700/LTE850/CDMA850/GSM900 sub-bands and boasts an impressive 37% −15 dB impedance bandwidth within the frequency range of 688-1000 MHz. The typical isolation between polarizations remains stable at 35 dB. Notably, the antenna demonstrates varying half-power beamwidths (HPBWs) of 55º-65º and 61º-66º in the elevation and azimuth planes, respectively, with a gain level of 7.85 ± 0.55 dBi. Additionally, the antenna provides sufficiently high front-to-back ratio (FBR) and cross-polarization discrimination (XPD) within the intended frequency band, making it an excellent candidate for practical base station implementations.

As summarized in Table 2, the prototyped antenna outperforms the studies in cited research especially by its wide impedance bandwidth, good isolation and small profile. The simulated and measured results show that the antenna is a good candidate for base station applications spanning 698-960 MHz band.

Table 2. *Comparison of related works*

[Ref.]	BW (MHz) %	Isolation ($\|S_{21}\|$,dB)	Height (mm)	FBR (dB)	XPD* (dB)
[4]	(800-960) 18.18% (S_{11}, $\|S_{22}\| < -14$ dB)	< –18	42	> 15	> 15
[5]	(806-960) 17.44% ($\|S_{11}\|$, $\|S_{22}\| < -15$ dB)	-	117	~ 0	> 17.5
[7]	(700-960) 31.30% ($\|S_{11}\|$, $\|S_{22}\| < -10$ dB)	< – 27	100	> 20	> 20
[8]	(790-960) 19.4% ($\|S_{11}\|$, $\|S_{22}\|$ < –15 dB)	< – 26	69	> 25	> 15
[10]	(698-960) 31.6% ($\|S_{11}\|$, $\|S_{22}\|$ < –12 dB)	< – 25	80	> 30	> 30
[11]	(790-980) 21.4% ($\|S_{11}\|$, $\|S_{22}\| < -14$ dB)	< – 30	85.1	> 25	> 25
[14]	(850-1010) 18.3% ($\|S_{11}\|$, $\|S_{22}\| < -15$ dB)	< – 30	62	> 30	> 18
This work	(688-1000) 37% ($\|S_{11}\|$, $\|S_{22}\| < -15$ dB)	< – 35	42.6	> 28	> 25

*: XPD levels are taken at boresight ($\theta = 0^o$)

CONFLICTS OF INTEREST

No conflict of interest was declared by the authors.

REFERENCES

[1] Mishra, P. K., Jahagirda, D. R., and Kumar, G., "A review of broadband dual linearly polarized microstrip antenna designs with high isolation [education column]", IEEE Antennas and Propagation Magazine, 56(6): 238–251, (2014).

[2] Luo, Y., Chu, Q. X., and Wen, D. L., "A ±45º dual-polarized base-station antenna with enhanced cross-polarization discrimination via addition of four parasitic elements placed in a square contour", IEEE Transactions on Antennas and Propagation, 64(4): 1514–1519, (2016).

[3] Ding, C., Sun, H., Ziolkowski, R. W., and Guo, Y. J., "Simplified tightly-coupled cross-dipole arrangement for base station applications", IEEE Access, 5: 27491–27503, (2017).

[4] Zhao, Y., Rakluea, C., Hongnara, T., and Chaimool, S., "A compact dual-broadband multiple-input multiple-output (MIMO) indoor base station antenna for 2G/3G/LTE systems", IEEE Access, 7: 82238–82245, (2019).

[5] Dai, X. W., Wang, Z. Y., Liang, C. H., Chen, X., and Wang, L. T., "Multiband and dual-polarized omnidirectional antenna for 2G/3G/LTE application", IEEE Antennas and Wireless Propagation Letters, 12: 1492–1495, (2013).

[6] Wen, H., Weng, Y., Qi, Z., Li, F., and Fan, J., "A Multiband Dual-Polarized Omnidirectional Antenna for 2G/3G/LTE Applications", in IEEE Antennas and Wireless Propagation Letters, 17(2): 180-183, (2018).

[7] Alieldin, A., Huang, Y., Boyes, S. J., Stanley, M., Joseph, S. D., Hua, Q., and Lei, D., "A triple-band dual-polarized indoor base station antenna for 2G, 3G, 4G and sub-6 GHz 5G applications", in IEEE Access, 6: 49209-49216, (2018).

[8] Cui, G., Zhou, S. G., Gong, S. X., and Liu, Y., "A compact dual-polarized antenna for base station application", Progress in Electromagnetics Research Letters, 59: 7-13, (2016).

[9] Zhou, S., Tan, P., and Chio, T., "Low-profile, wideband dual-polarized antenna with high isolation and low cross polarization", IEEE Antennas and Wireless Propagation Letters, 11: 1032-1035, (2012).

[10] He, Y., Yue, Y., and Shen, Z., "A novel broadband dual polarized antenna element for LTE700 MHz/GSM850 MHz/GSM900 MHz applications", IEEE Access, 4: 4321-4326, (2016).

[11] Kaboli, M., Mirtaheri, S. A., and Abrishamian, M. S., "High-isolation X-polar antenna", IEEE Antennas and Wireless Propagation Letters, 9: 401-404, (2010).

[12] Kaboli, M., Abrishamian, M. S., Mirtaheri, S. A., and Aboutorab, S. M., "High-isolation XX-polar antenna", IEEE Transactions on Antennas and Propagation, 60(9): 4046-4055, (2012).

[13] White, C. R., Rebeiz, G. M., "A differential dual-polarized cavity-backed microstrip patch antenna with independent frequency tuning", IEEE Transactions on Antennas and Propagation, 58 (11): 3490-3498, (2010).

[14] Lau, K. L., Luk, K. M., and Lin, D., "A wide-band dual-polarization patch antenna with directional coupler", IEEE Antennas and Wireless Propagation Letters, 1: 186-189, (2002).

[15] Ciydem, M., "Wideband dual polarized antenna", Journal of the Faculty of Engineering and Architecture of Gazi University, 29(4): 817-821, (2014).

[16] Ciydem, M., "Isolation enhancement in wideband dual-polarised suspended plate antenna with modified T-type probes", Electronics Letters, 50(5): 338-339, (2014).

[17] Ciydem, M., Koc, S., "High isolation dual-polarized broadband antenna for base stations", Microwave and Optical Technology Letters, 57(3): 603-607, (2015).

[18] Ciydem, M., Miran, E. A., "Dual-polarization wideband sub-6 GHz suspended patch antenna for 5G base station", IEEE Antennas and Wireless Propagation Letters, 19(7): 1142-1146, (2020).

[19] Abbosh, M., "Ultra wideband vertical microstrip-microstrip transition", IET Microwaves, Antennas and Propagation, 1(5): 968–972, (2007).

[20] Ciydem, M., "A Low-Profile Dual-Polarized Antenna with High Isolation and High Front-to-Back Ratio for 5G Base Stations", The Applied Computational Electromagnetics Society Journal (ACES), 36(9): 1229-1236, (2021).

[21] Miran, E. A., Ciydem, M., "Dual-polarized elliptic-H slot-coupled patch antenna for 5G applications", Turkish Journal of Electrical Engineering and Computer Sciences, 30(4): 1204-1218, (2022).